# Electronic Supporting Information

## Self-activated continuous pulverization film: an insight into the mechanism of extraordinary long-life cycleability of hexagonal $H_{4.5}Mo_{5.25}O_{18}\cdot(H_2O)_{1.36}$ microrods†

Zihua Li,[ab] Hai Wang,[*ab] Zhuangzhi Sun, [ab] Jian Su, [ab] Zuyun Wang [c] and Linjiang Wang[ab]

[a]College of Materials Science and Engineering, Guilin University of Technology, Guilin 541004, China

[b]Key Laboratory of New Processing Technology for Nonferrous Metals and Materials, Ministry of Education, Guilin University of Technology, Guilin 541004, China

[c]College of Civil Engineering and Architecture, Guilin University of Technology, Guilin 541004, China

* To whom correspondence should be addressed.

Tel: +86-773-5896-672. Fax: +86-773-5896-671. E-mail:hbwanghai@gmail.com (H Wang).

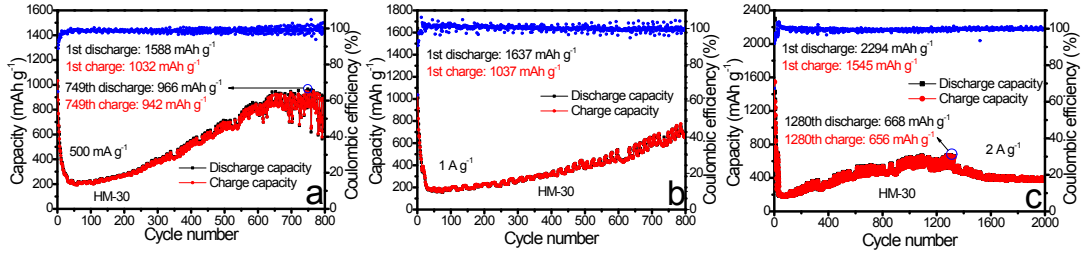


**Fig. S1** The cycling performance and Coulombic efficiency of HM-30 at 500 mA $g^{-1}$ (a), 1 A $g^{-1}$ (b) and 2 A $g^{-1}$ with different cycles, respectively.

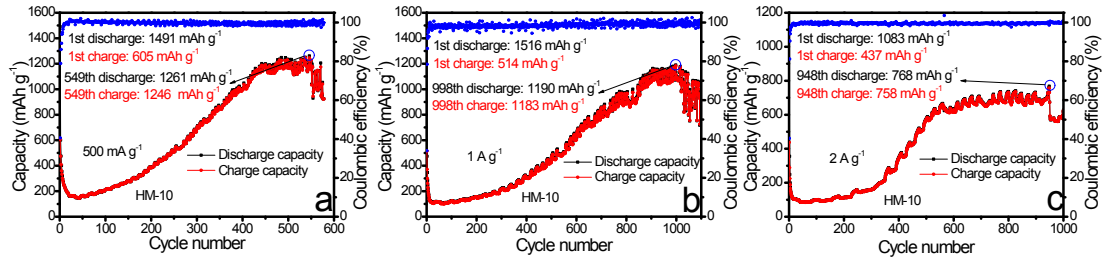


**Fig. S2** The cycling performance and Coulombic efficiency of HM-10 at 500 mA $g^{-1}$ (a), 1 A $g^{-1}$ (b) and 2 A $g^{-1}$ with different cycles, respectively.

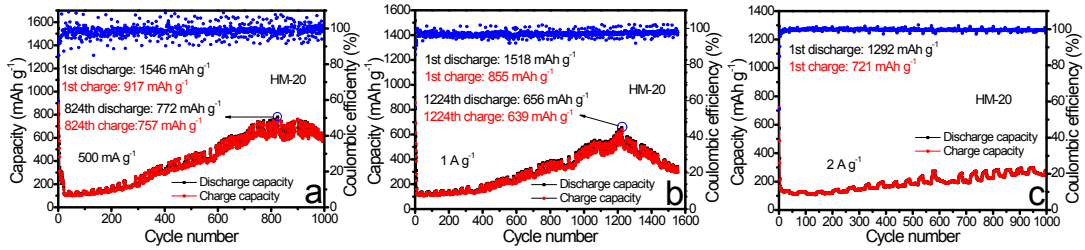


**Fig. S3** The cycling performance and Coulombic efficiency of HM-20 at 500 mA $g^{-1}$ (a), 1 A $g^{-1}$ (b) and 2 A $g^{-1}$ with different cycles, respectively.

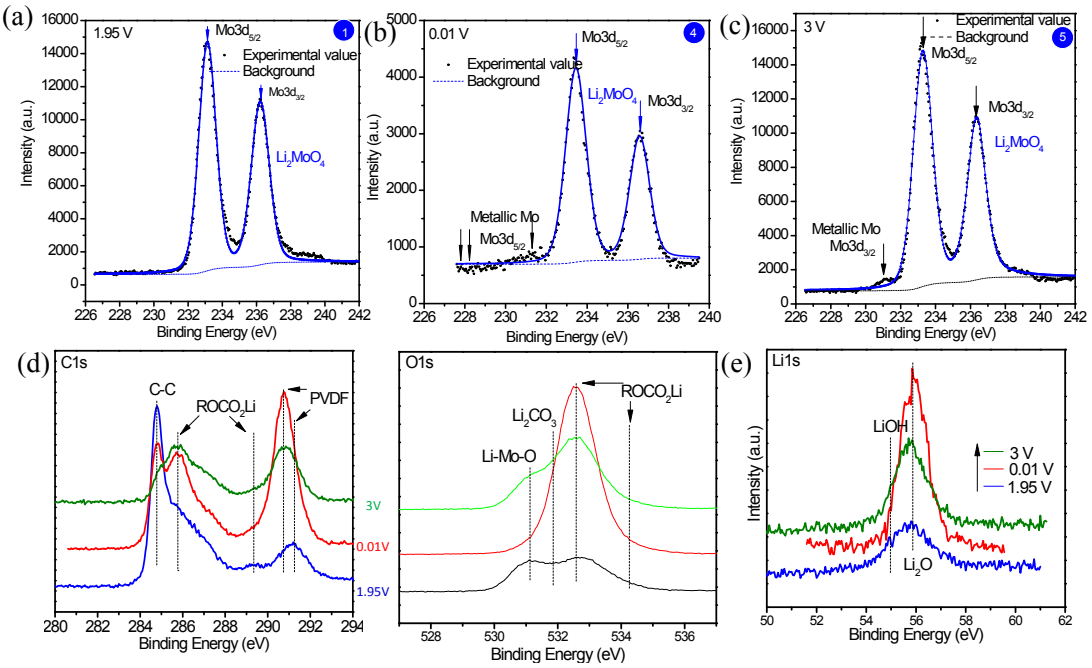


**Fig. S4** XPS spectra of HM-30 microrods electrodes discharged to 1.95V, 0.01V and charged to 3V; (a)-(c) Mo3d , (d) C1s, O1s and (e) Li1s in the first cycle.

To real the presence of Mo and $Li_2O$ within amorphous cage, we have performed the XPS characterization of the three samples at different charge-discharge stages ①, ④ and ⑤, corresponding to 1.95, 0.01 and 3 V, respectively (See Fig. 2a). For the sample at 0.01 V (④), it is found that there are three satellite peaks at 227.8, 228.2, and 231.3 eV with low intensity, as shown in Fig. S4(b), which is characteristic of metallic Mo. The results show that the formation of metallic Mo is at the end of discharge. These low intensity peaks may be due to the presence of amorphous spheres. This can be reasonably inferred from the HRTEM (Fig. 5) and C1s and O1s (Fig. S4(d)). Surprisingly, for the sample at 3 V (⑤), a metallic Mo peak at 231.3 eV ($3d_{5/2}$) is also observed (Fig. S4(c)), corresponding to the end of the charge, indicating that the partial conversion reaction metallic Mo to $Li_{2+x}Mo_yO_z$. The residual metal Mo will be continuously activated with charge and discharge within the amorphous spheres. Therefore, the specific capacity of HM-30 first decreased then increased gradually. These unique phenomena also appeared in other previous literature. At the end of 1000$^{th}$ charge, Mo will be consumed gradually till it was completely consumed. Actually, metallic Mo could not also be observed in previous literature. Therefore, the fact of metal Mo could not be observed from HRTEM (Fig. 5) is easy to understand based on conversion reaction equation 4. XPS investigation at different charge-discharge stages provided a strong evidence of the presence of Mo.

Furthermore, we also found that a strong evidence of Li1s state of $Li_2O$ from the three samples (Fig. S4(e)).

All the above results validate the proposed mechanism of step II.

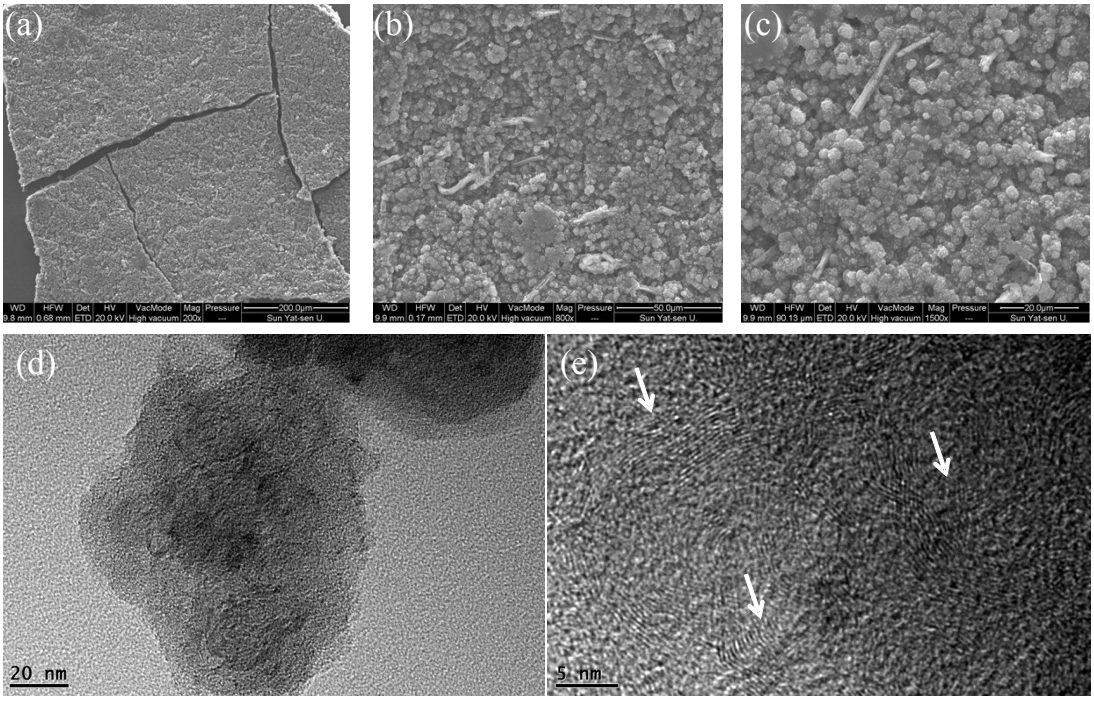


**Fig. S5** FESEM images of another batch of HM-30 sample after 1000$^{th}$ cycles with different magnification (a)-(c) and TEM images of $Li_2MoO_4$ nanowire clusters encapsulated within amorphous cages. (d) low-magnification TEM image; (e) high-magnification TEM image (white arrows).

In the low-magnification FESEM image can reveal that the HM-30 microrods electrodes was transformed into a robust gel-like thin film. Subsequently, in the high-magnification FESEM image, we can find that the robust gel-like thin film is composed of large amounts of uniform spheres. It is accordance with (d) low-magnification TEM image.（e）high-magnification TEM image reveals that some nanowires clusters were encapsulated within the amorphous spheres. The ultrathin nanowire was further verified to be $Li_2MoO_4$ from the HRTEM result, which is agreed with the XRD results, as shown in Fig. 3.

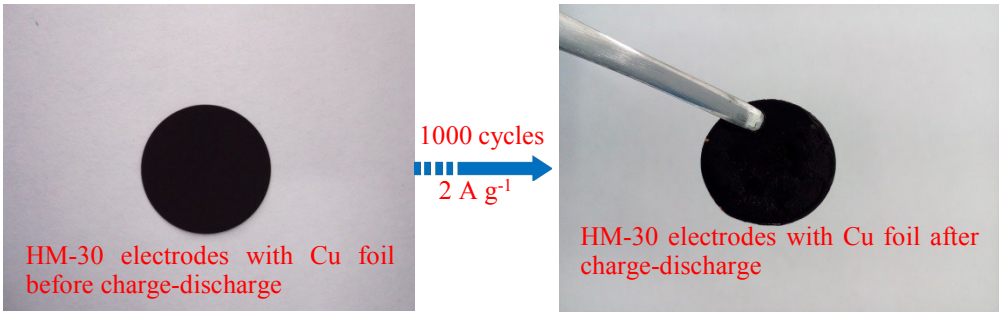


**Fig. S6** The comparison of the HM-30 before and after charge-discharge at 1000$^{th}$ cycles at a high current density of 2 A g$^{-1}$.

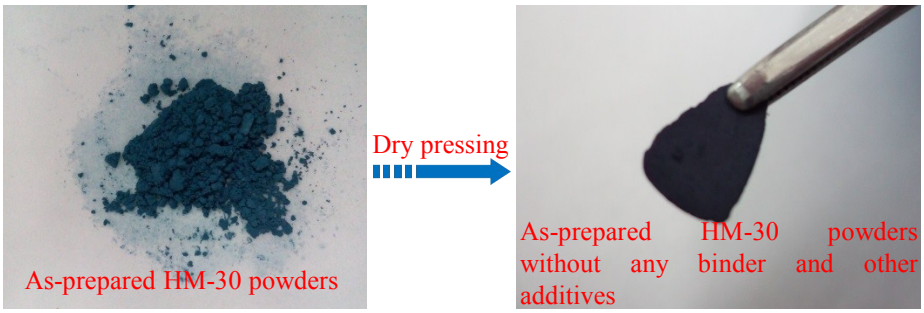


**Fig. S7** The comparison of the HM-30 before and after dry pressing.

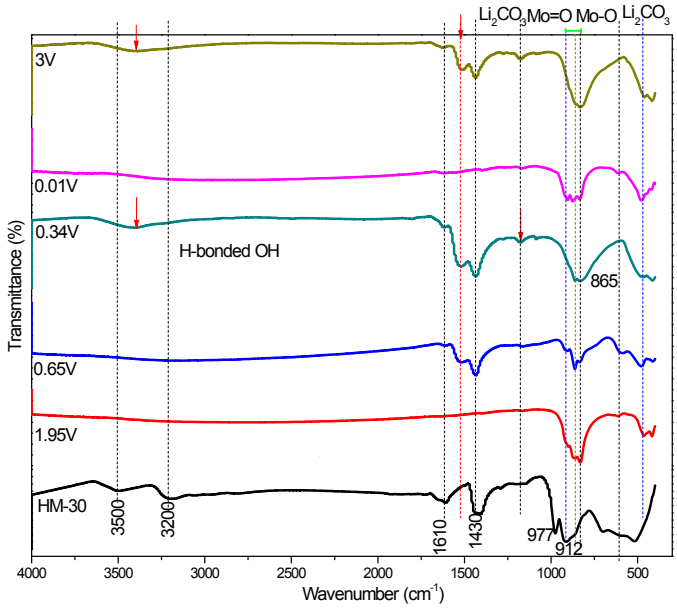


**Fig. S8** The corresponding ex-situ FTIR spectra of HM-30 and different charge and discharge process at 1st cycle (Fig. 2).

**Tab. S1 Comparative results of the lattice parameters and unit cell volume between hexagonal $H_{4.5}Mo_{5.25}O_{18}\cdot(H_2O)_{1.36}$ and rhombohedral $Li_2MoO_4$.**

| As-synthesized oxide | After lithiation | % volume change |
|---|---|---|
| $H_{4.5}Mo_{5.25}O_{18}\cdot(H_2O)_{1.36}$ a=10.584, c=3.7278 Å, Volume=361.15 Å$^3$ | $Li_2MoO_4$ a=14.3368, c=9.5889 Å, Volume=1706.88 Å$^3$ | (1706.88-361.15)/361.15=372.6% |

**Tab. S1** presents the changes of lattice parameters and unit cell volume of two different crystal phases of $H_{4.5}Mo_{5.25}O_{18}\cdot(H_2O)_{1.36}$ and $Li_2MoO_4$. The lithiation of $H_{4.5}Mo_{5.25}O_{18}\cdot(H_2O)_{1.36}$ results in a 2.0 Li/Mo ratio in $Li_2MoO_4$. Obviously, the insertion amount of lithium ion in $H_{4.5}Mo_{5.25}O_{18}\cdot(H_2O)_{1.36}$ is large, due to its ample space considering its large tunnel dimension 3.5 Å in diameter. It should be noted that the large amounts of lithium ion is important prerequisites for the design of various electrode materials with high specific capacity in LIBs.. It should be noted that the amount of insertion lithium is considerably higher than other anode materials, for example, 4.4 Li for $SnO_2$, 6.0 for $Fe_2O_3$ and 2.0 for CoO. It is no doubt that HM is a potential anode material for LIBs application. However, the volume expansion of $H_{4.5}Mo_{5.25}O_{18}\cdot(H_2O)_{1.36}$ after lithiation cannot be ignored. In our case, the conversion reaction of $H_{4.5}Mo_{5.25}O_{18}\cdot(H_2O)_{1.36}$ into $Li_2MoO_4$ corresponds to 372.6% volume expansion upon lithium insertion, as shown in Tab. 1. The aim of our work is to how to solve the problem of capacity fading caused by the volume changes.

**Tab. S2 The performance comparison of three samples, HM-10, HM-20 and HM-30 under different current density.**

| samples | 500 mA $g^{-1}$ | 1 A $g^{-1}$ | 2 A $g^{-1}$ |
|---|---|---|---|
| HM-10 | 1217 mAh $g^{-1}$ ($550^{th}$) | 947 mAh $g^{-1}$ ($800^{th}$) | 624 mAh $g^{-1}$ ($800^{th}$) |
| HM-20 | 473 mAh $g^{-1}$ ($550^{th}$) | 381 mAh $g^{-1}$ ($800^{th}$) | 251 mAh $g^{-1}$ ($800^{th}$) |
| HM-30 | 710 mAh $g^{-1}$ ($550^{th}$) | 670 mAh $g^{-1}$ ($800^{th}$) | 496 mAh $g^{-1}$($1000^{th}$) |

Tab. S2 reveals that HM-10, HM-20 and HM-30 exhibit the same cycling performance trend at different current densities. At the same current density, the charge-discharge capacity of the three electrode materials followed such order, HM-10> HM-30> HM-20.

As LIBs anode materials, all the three samples show good and stable cycle performance. At the beginning, we choosed HM-30 as our first research object. Moreover, HM-30 can prove "damage-reconstruction" new ideas we proposed, so we select the HM-30 as our first object. As further deeper investigation continues, we discovered that HM-10 exhibit best performance among HM-10, HM-20 and HM-30. Further research will reveal the relationship between the aspect ratio and performance.

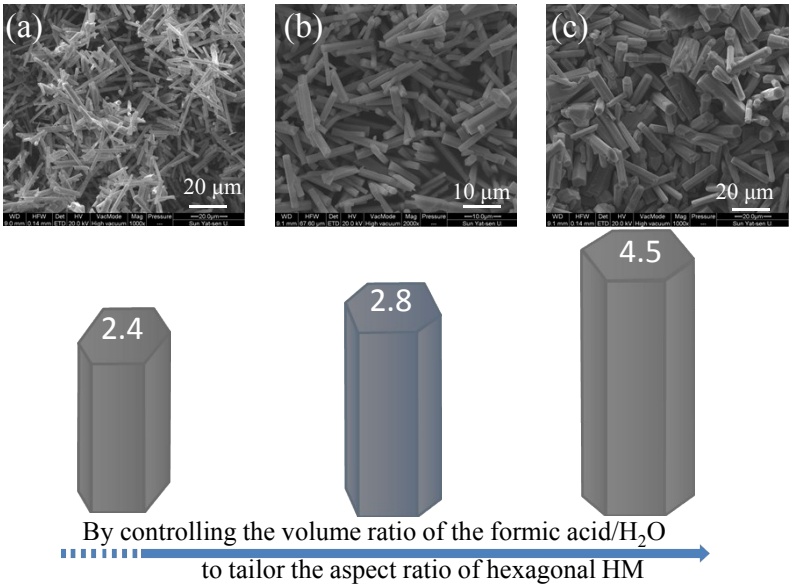


**Scheme. S1** (a) Schematic illustration of the procedure used to prepare one-dimensional hexagonal HM with different aspect ratio, 2.4, 2.8 and 4.5; (b) the corresponding FESEM images of HM-10 (a), HM-20 (b) and HM-30 (c).

Different properties are often determined by different aspect ratio of hexagonal microrods. In our case, we found that the aspect ratio of hexagonal HM is determined by the volume ratio of the formic acid/$H_2O$. It is easily observed that the aspect ratio of HM increased with the increase of volume ratio of formic acid/$H_2O$, as shown in Scheme. S1. Additionally, a similar increase trend of the diameter of HM is also observed.

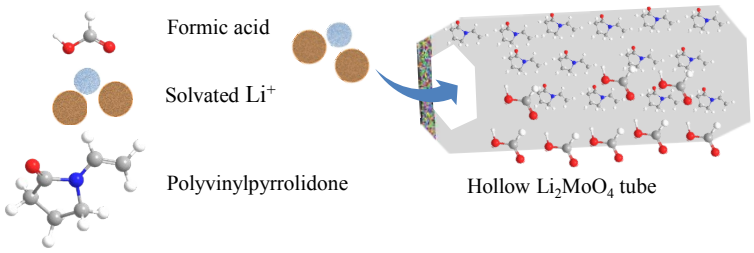


**Scheme. S2** The schematic illustration of solvated $Li^+$ insertion hollow $Li_2MoO_4$ tube.

The solvated lithium ion was reasonably inferred to insert into hollow $Li_2MoO_4$ tube and then to insert wide one-dimensional tunnel, due to the damage of nanotube microstrcture and lattice expansion of $Li_2MoO_4$ with cycles.

**Supplementary Note 1| The discussion of the advantages of pulverization process**.

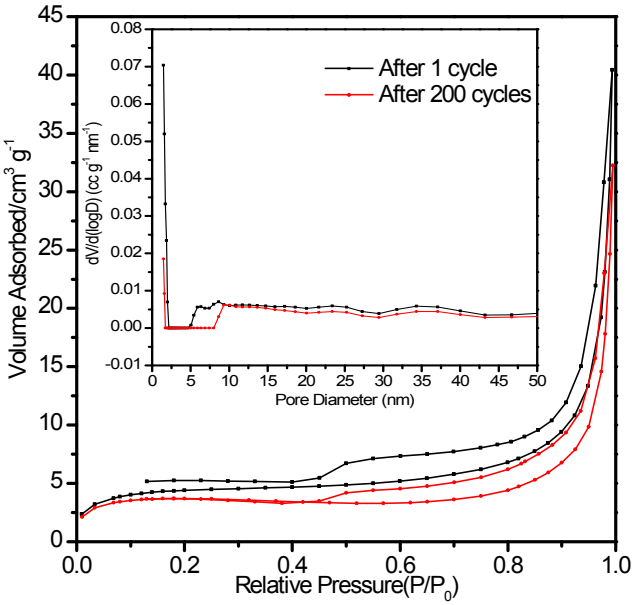


**Fig. S9** Nitrogen adsorption-desorption isotherms of HM-30 microrods electrodes after 1st and 200th cycles. The inset shows the corresponding BJH pore-size distribution plots. The nitrogen-sorption analysis reveals that the BET specific surface area of HM-30 are 15.56 (after 1st cycle) and 12.77 $m^2/g$ (after 200th cycles), correspondingly, the pore volume are 0.003176 $cm^3/g$ for 1st cycle and 0.004327 $cm^3/g$ for 200th cycles. Some micropore ranging from 1 to 2 nm exist in the two typical samples.

To better address the advantages of pulverization process, which would lead to enhance specific surface area, as proposed in our manuscript, we performed the BET measurements of the two typical samples at different stages (after 1st cycle and after 200th cycles). Unfortunately, we can not obtain satisfactory results as we expected. The BET specific surface area of is 15.56 (after 1st cycle) and 12.77 $m^2/g$ (after 200th cycles), respectively. We think that the pulverized powders were embedded in the continuous film based on the observation of FESEM (Fig. 4c), and we also found that very litter void was exposed. Therefore, such a low specific surface area is understandable. This also can get explanations from the low pore volume (micropore volume, 0.003176 $cm^3/g$ for 1st cycle, 0.004327 $cm^3/g$ for 200th cycle). Generally speaking, the relative large pore volume will lead to high specific surface area [1-4]. From another point of view, this also gave new evidence of the formation of robust continuous film.

Very recently, we also noted that Yang-Kook Sun et al., reported a physical pulverization strategy for preparing a highly active composite of $CoO_x$, indicating the advantages of electrode materials pulverization [5]. In our case, unlike pulverized CoOx [5], our pulverized powder was encapsulated within amorphous spheres.


1. C. Wang, Y. Zhou, M. Y. Ge, X. B. Xu, Z. L. Zhang and J. Z. Jiang, *J. Am. Chem. Soc.*, 2010, **132**, 46-47.
2. J. S. Chen, T. Zhu, X. H. Yang, H. G. Yang and X. W. Lou, *J. Am. Chem. Soc.*, 2010, **132**, 13162-13164.
3. Z. X. Li, F. B. Shi, Y. Ding, T. Zhang and C. H. Yan, *Langmuir*, 2011, **27**, 14589-14593.
4. R. Demir-Cakan, M. Morcrette, F. Nouar, C. Davoisne, T. Devic, D. Gonbeau, R. Dominko,

C. Serre, G. Ferey and J. M. Tarascon, *J. Am. Chem. Soc.*, 2011, **133**, 16154-16160.
5. J. Ming, W. J. Kwak, J. B. Park, C. D. Shin, J. Lu, L. Curtiss, K. Amine and Y. K. Sun, *ChemPhysChem*, 2014, **15**, 2070-2076.

It should be noted that it is still very hard for us to obtain real specific surface area of the pulverized inorganic materials because the pulverized powders themselves are composites of inorganic and organic composition. Although we have repeatedly washed the powders with organic solvent DMC for many times, it is difficult to guarantee to obtain the pure inorganic powders.

Recently, we are also exploring to how to obtain higher specific surface area of other electrode materials via lattice volume expansion of electrode materials via a simple synthesis method. It should be emphasized that the pulverized powders are not obtained via charge-discharge process. In our case (HM-30), it is transferred to $Li_2MoO_4$ via charge-discharge process. Microrods were evolved to nanowire clusters, previous literature showed that the specific surface area of the nanowire clusters is higher than that of microrods [1-3].

1. J. R. Huang, G. J. Fu, C. C. Shi, X. Y. Wang, M. H. Zhai and C. P. Gu, *J. Phys. Chem. Solids*, 2014, **75**, 1011-1016.
2. N. N. Wang, X. J. Ma, Y. P. Wang, J. Yang and Y. T. Qian, *J. Mater. Chem. A*, 2015, **3**, 9550-9555.
3. L. M. Leng, X. Y. Zeng, H. Y. Song, T. Shu, H. S. Wang and S. J. Liao, *J. Mater. Chem. A*, 2015, **3**, 15626-15632.